Morton

ICIASF '81

RECORD

International Congress on Instrumentation in
Aerospace Simulation Facilities

PLPRINT

IN-36-TM

0:46×3

Dayton, Ohio
September 30, 1981

APPLICATION OF A LASER INTERFEROMETER SKIN-FRICTION METER IN COMPLEX FLOWS

by D. J. MONSON, D. M. DRIVER, AND J. SZODRUCH

Ames Research Center, NASA, Moffett Field, California 94035

Summary

A nonintrusive skin-friction meter has been found useful for a variety of complex wind-tunnel flows. This meter measures skin friction with a remotely located laser interferometer that monitors the thickness change of a thin oil film. Its accuracy has been proven in a low-speed flat-plate flow. The wind-tunnel flows described here include subsonic separated and reattached flow over a rearward-facing step, supersonic flow over a flat plate at high Reynolds numbers, and supersonic three-dimensional vortical flow over the lee of a delta wing at angle of attack. The data-reduction analysis was extended to apply to three-dimensional flows with unknown flow direction, large pressure and shear gradients, and large oil viscosity changes with time. The skin friction measurements were verified, where possible, with results from more conventional techniques and also from theoretical computations.

Key words: skin friction — boundary layers — non-intrusive laser interferometer — wind-tunnel instrumentation.

NOMENCLATURE

A = dT/dt [see Eq. (A3)]

B = $\partial\tau/\partial s$ [see Eq. (A2)]

C = $\partial\tau/\partial n$ [see Eq. (A2)]

C_f = local skin-friction coefficient, τ/q

dp/dx = external-flow pressure gradient

g = gravitational acceleration

H = step height

i = laser beam incidence angle measured from the normal to a surface

M = Mach number

N = fringe number

n = coordinate perpendicular to oil-flow direction (see Fig. 8)

n_o = oil index of refraction

q = free-stream dynamic pressure

R_L = Reynolds number based on model length

r = laser beam refraction angle within oil measured from the normal to a surface

S = oil-viscosity/temperature-slope [see Eq. (A4)]

s = coordinate along oil-flow direction (see Fig. 8)

T = temperature

t = time

$\bar{U}_{REF}$ = tunnel reference speed

x = coordinate parallel to line joining beams (see Fig. 8); also, distance downstream from step

Y_o = tunnel height

y = oil thickness

z = coordinate perpendicular to line joining beams (see Fig. 8)

α = tunnel-wall deflection angle; also, delta-wing angle of attack

β = shear-stress gradient correction parameter [see Eq. (A10)]

γ = local oil-flow angle with respect to the x coordinate (see Fig. 8)

ΔN = incremental change in fringe number

Δt = incremental change in time

Δx = beam spacing

δ_{BL} = boundary-layer thickness

ϵ = pressure gradient and gravity-correction parameter [see Eq. (A11)]

θ = surface inclination from horizontal

λ = laser wavelength

ν = oil kinematic viscosity

ρ = oil density

τ = local skin friction

Superscripts

$(\;)'$ = corrected or "effective" value

$(\bar{\;\;})$ = average value

Subscripts

R   = reattachment length

x,z   = directions as shown in Fig. 8

1,2   = refer to positions in Fig. 8 or to times in Fig. 9

∞ = free-stream conditions

θ = momentum thickness

1. INTRODUCTION

The importance of data on skin friction in aerodynamic testing has stimulated a continuing effort to develop reliable instrumentation for its measurement. Traditional devices such as floating-element balances, Preston tubes, pitot tubes combined with the use of a Clauser chart, and surface thin-film heat-transfer gauges, remain in wide use. However, all are seriously limited in one or more aspects: for example, they measure skin friction only indirectly, are applicable to a limited range of flow conditions, are delicate and tedious to use, require permanent installation, or they are intrusive to the flow [1].

Recently, a two-beam laser-interferometer technique has been developed that overcomes many of the above limitations. The details of the optical arrangement for the instrument and its preliminary application are fully described in Ref. 2. To date its validity has been proven in a low-speed flat-plate boundary layer.

Basically, the instrument is an improved version of an earlier one developed by Tanner and Blows [3] and Tanner [4] to measure skin friction by monitoring the thickness change of an oil film subject to shear stress. The technique provides a direct nonintrusive skin-friction measurement that is simple and has the potential of being used in a wide variety of complex flows.

This paper describes the application of the two-beam laser-interferometer to several types of complex flows to further define its usefulness and limitations for a wide range of aerodynamic situations. Included are subsonic separated and reattached flows over a rearward-facing step, supersonic flow over a flat plate at high Reynolds numbers, and supersonic three-dimensional vortical lee flow over a slender delta wing at angle of attack. Application of the method in the above flows tests its validity in the presence of additional complexities such as large

pressure gradients, shear gradients, and wall-temperature changes with time.

In the following sections, we also present the derivation of the data-reduction equations that include corrections for all of the described effects. The skin-friction measurements obtained are compared with those from more conventional techniques where possible, or with theoretical calculations. Finally, we discuss practical suggestions for using the method, certain problems and limitations that were discovered during the tests, and several possibilities for improving the instrument in the future.

2. PRINCIPLE

The basic idea of the skin-friction meter is to measure precisely the rate of change of thickness of an oil film subject to shear stress using a laser so that oil-flow theory can be applied to deduce skin friction. In the preferred method, two laser beams with known spacing are focused at points on an oil film behind the leading edge of the film. A portion of each beam reflects from the oil as well as from the substrate, and these signals are recombined on a photodiode. Because of the coherence and narrow spectral width of the beams, they produce a modulation in recorded intensity that corresponds to a change in the integer number of wavelengths equal to the oil thickness. The recorded fringe time records can be used to infer the time rate of change in oil thickness and its slope. This information can, in turn, be related to the average skin friction during the run. The data-reduction analysis and procedure, including corrections for pressure and shear gradients, oil viscosity changes with time, and gravity, is detailed in Appendix A.

For the present tests, the skin-friction meter consisted of a separate transmitter and receiver attached to optical rails on separate adjustable free-standing tripods for flexible positioning. The two beams produced by the transmitter were orthogonally polarized so that their signals could be separated at the receiver by a polarization beam splitter. The He-Ne laser wavelength was 6328 Å and the power in each beam was attenuated to about 0.2 mW to avoid heating the oil. The oil properties required in the data reduction were obtained from Dow Corning product literature. The required oil viscosity was determined from the test surface temperature, as measured by a thermocouple embedded in the back side. A more detailed description of the instrument and method is given in Ref. 2.

Although we intended to use the two-beam skin-friction method in these experiments, this was not possible because of limited optical access into the two test wind tunnels. Since both only had side windows, we were forced to bring the laser beams into the test sections at incidence angles between 40° and 55°. This caused the beam, with its polarization aligned normal to the surface, to approach Brewster's angle, leading to an impractically low reflection from the oil surface. The eventual solution of this problem was to bring the beams in at a grazing incidence angle to the model. This technique is discussed in Appendix B. Unfortunately, we discovered the solution too late to allow use of the two-beam method for this work. Consequently, we

were forced to resort to the original single-beam method of Tanner [4] as a temporary but less accurate method. In that method, the forward beam with known spacing from the rear beam is simply used to visually locate the oil leading edge before a run. The beam is judged to be on the leading edge at the point where a transition from a single to a double reflection is observed [4]. The data-reduction equations in Appendix A are simplified for the single-beam method because the product $N_2' t_2'$ becomes zero, and Δx equals the distance from point (1) to the oil leading edge.

3. RESULTS AND DISCUSSION

3.1 Separated and Reattached Flow

Measurements of skin friction were first performed in a separated and reattached flow behind a rearward-facing step, using the High Reynolds Number Pilot Channel at Ames Research Center. This facility is a small, subsonic, continuous-running tunnel that draws in filtered room air and discharges it into large vacuum spheres. The test-section geometry and test conditions are shown in Fig. 1. The top wall is adjustable to positive or negative angles to vary the free-stream pressure gradient and thereby alter the reattachment length behind the step.

The laser interferometer was used to measure skin friction at several locations in the region of attached flow ahead of the step and throughout the separated and reattached regions downstream of the step for top-wall deflection angles of 0° and 6°.

The two-dimensional nature of the flow and constant oil temperature allowed a simplified version of the data-reduction equations from Appendix A to be used. In particular, the constants A, C, γ, and θ could all be set to zero. Pressure-gradient corrections were applied from measured pressure distributions on the lower tunnel wall. Shear-stress gradient corrections along the flow direction were applied, using the simplified method described following Eq. (A12).

The measured skin-friction coefficients are shown in Fig. 2a for zero wall-deflection angle. The C_f term is defined as the skin friction divided by the reference free-stream dynamic pressure measured just upstream of the step. The error bars on the interferometer data represent limits of 95% confidence; they are assessed using an rms uncertainty analysis [5] that combines the computed uncertainty of all the variables used in the data-reduction equations with the scatter of up to 2 to 10 repeat measurements at each axial station. Runs were made using silicon oils with nominal viscosities of 10, 50, or 200 centistokes (cS), depending on the level of shear encountered. The data are compared with Preston-tube [1] and "law-of-the wall" [1] skin-friction measurements at $x/H = -4$ and 36; excellent agreement is found. These experimental methods are not valid in the separated and near-attached regions. However, the data are compared in those regions with a recent theoretical calculation by Sindir [6], using the Navier-Stokes equations combined with an algebraic eddy-viscosity turbulent shear-stress model. Sindir's calculation is in fair qualitative agreement with the interferometer data in the separated and reattached

regions. Although the prediction does a fairly good job of locating reattachment, it tends to underpredict the magnitude of skin friction in those regions.

The interferometer skin-friction data in Fig. 2a show excellent repeatability and apparent self-consistency over the entire range of distances tested. Even repeat runs in which the oil viscosity varied from 10 to 200 cS were very repeatable and consistent. A point of special interest is that we were able to measure, with good repeatability, the very low skin friction occurring in the small corner eddy region at the base of the step. This illustrates how the method can measure small-scale flow details, as well as very low levels of skin friction, simply by using low-viscosity oil. Notice that Sindir's calculation completely fails to predict the corner eddy for this case.

We had expected difficulty with the oil-flow method close to the reattachment point because of the combined effects of low shear stress, large pressure gradients, and flow fluctuations. However, we were able to successfully measure skin friction very near to the mean reattachment line by using the more viscous (200 cS) oil to damp out the fluctuations, and by making long runs to obtain enough fringes. Although the percentage error is higher for the data near reattachment, the absolute error is small because of the low shear stress there.

The pressure gradients for the 0° case were largest at the reattachment location and resulted in up to a 10% correction to skin friction there and at nearby points. The correction for all other regions was negligible. The shear-stress gradient correction to the data was as large as 8% in the separated region, and negligible elsewhere.

The measured skin friction is shown in Fig. 2b for an upper-wall deflection angle of 6°. This geometry provides a superimposed adverse pressure gradient on the flow. The interferometer data once again show good repeatability and self-consistency over the range of axial station measured, and are in excellent agreement with the Preston tube and law-of-the-wall measurements. The data show that deflecting the wall lengthens the separated region and reduces the skin friction in all regions except upstream of the step at $x/H = -4$. The comparison with Sindir's calculation is somewhat better for this case than that for $\alpha = 0°$, except that the reattachment length is now underpredicted by 13%. Again, Sindir's calculation does not predict the corner eddy at the base of the step. These data and those for $\alpha = 0°$ demonstrate the ability of the skin-friction meter to measure subtle skin-friction details in complex separated flows and to do so with apparent accuracy.

The data in Figs. 2a and 2b also provide an accurate measurement of the mean reattachment length. The measurements of skin friction at locations slightly upstream and downstream of reattachment were linearly interpolated to find the point of zero shear (i.e., reattachment). A conventional method of locating reattachment in separated flows has been to observe the position where a liquid, such as alcohol, changes flow direction on the surface. There is a possibility of error with that method, however, because shear is zero at reattachment and the liquid flow direction may be dominated by the external-flow pressure gradient. The conventional

method was found to bracket the measurement of reattachment by the skin-friction meter in a comparison made for zero wall-deflection angle. However, the skin-friction meter allowed reattachment to be located more precisely.

Measurements of reattachment lengths, using the laser interferometer at several additional wall angles, are shown in Fig. 3, where they are compared with Sindir's calculations. One can see that theory and experiment are in fair agreement for small wall deflection angles, but the agreement becomes increasingly poor at larger angles. Uncertainty of each reattachment measurement was assessed based on the uncertainty of measuring skin friction. The increased uncertainty indicated by the error bars at large deflection angles is a result of severe flow fluctuations.

3.2 Supersonic High Reynolds Number Flow

The second test of the skin-friction meter was its application to the supersonic high Reynolds number flow on the wall of the High Reynolds Number Channel I at Ames Research Center. The tunnel is a variable-temperature blowdown facility designed for operation at reservoir pressures up to 30 atm. Rectangular nozzles with a test-section size of 25×38 cm that operate at $M_\infty = 2$ and 3 were used. Optical access required a beam incidence angle of about 50°, again requiring the use of a single-beam method. This presented a new problem because once we set the front beam on the oil leading edge, the oil continued to slowly spread, but tunnel operating procedures required a delay in starting of several minutes. A solution was to prethin the oil to minimize further spreading by wiping it once with a rubber squeegee.

The skin friction for these cases was computed by the method given in Appendix A, with only the correction for variable wall temperature required. A thermocouple in the tunnel wall measured linear temperature changes of up to 10° C for some runs.

The measured skin-friction results are shown in Fig. 4 for $M_\infty = 2$ and 3 over a range of Reynolds number (Reynolds number was changed by varying tunnel stagnation pressure, and is based on the length to the nozzle throat). The error bars show the scatter between two or more repeated measurements at each Reynolds number. Nominal oil viscosity was 1,000 or 3,000 cS, depending on the pressure. The data are compared with calculations using a reliable turbulent boundary-layer code [7]. They are observed to agree with the computations within ±10% at both Mach numbers over the Reynolds number range tested. Although this agreement demonstrates the utility of the oil-flow skin-friction method in supersonic flow, the accuracy of the results is less than that (about ±5%) achieved in previous tests [2] in low-speed and lower-Reynolds-number flow. Possible causes of the reduced accuracy are discussed in Sec. 3.4.

Problems were also encountered when attempting to measure skin friction at very high shear levels, that is, at levels corresponding to Reynolds numbers above the maximum of 1×10^8 shown for the data in Fig. 4. High shear levels produced turbulent surface waves on the oil that persisted until the oil was quite thin. The problem grew worse with increased shear stress (i.e., increased stagnation pressure), until, at Reynolds numbers above the 1×10^8 maximum shown in Fig. 4, no useful fringe records could be obtained within the test time available. For example, at the highest Reynolds number shown in Fig. 4, only four useful fringe peaks were recorded. Nevertheless, successful measurements of skin friction have been obtained here at 120 N/m², or 40 times higher than the previous maximum demonstrated for this method [2].

3.3 Supersonic Three-Dimensional Flow

The final test of the skin-friction meter in this series of experiments was its application to the flow produced by the Ames High Reynolds Number Channel I on the lee of a 70° swept delta wing at angle of attack. This is a severe test of the method because of the complex flow over the wing. The general features of the flow are sketched in Fig. 5. Typically, it is characterized by a primary vortex separation at the leading edge, a reattachment farther inboard, and a secondary vortex separation within the primary vortex. Strong surface cross-flow exists between the primary attachment line and the secondary separation line, and the skin friction would be expected to vary significantly along the span from the wing centerline to the leading edge. Further details of this flow are given by Szodruch [8].

Tests on the delta wing were run at $M_\infty = 2$ and 3, and at angles of attack of 0° and 8°. All tests at both Mach numbers were performed at a fixed Reynolds number of 2.0×10^6 based on model length. Stagnation pressure was 0.7 and 1.2 atm at $M_\infty = 2$ and 3, respectively. Laser interferometer skin-friction measurements were performed at several spanwise locations 13 cm behind the tip of the 21-cm-long delta wing. All tests were performed using 1,000 cS viscosity oil. The axial skin-friction component was measured according to the procedure for three-dimensional flow outlined in Appendix A. To achieve this, the line defined by beam impingement points on the model surface was aligned parallel to the model axis, and the oil leading edge was applied perpendicular to the axis. The test and data-reduction procedures were the same as for the tunnel-wall tests. No corrections were applied for pressure or shear gradients.

Early in the delta-wing tests, we discovered that fringes in the film of oil after a run could be clearly observed by eye. Tanner and Blows [3] have shown that the spacing of such fringes is proportional to the local skin friction. Thus, by applying a line of oil across the wing, we could observe a qualitative picture of the spanwise skin-friction distribution. Two postrun photographs of such oil patterns for the wing at 8° angle of attack are shown in Figs. 6a and 6b for $M_\infty = 2$ and 3, respectively (the quality of the fringes in the photographs is far inferior to what can visually be observed immediately after a run). The figures show very complex skin-friction patterns across the span. In both cases, the centerline region exhibits a fine saw-tooth structure caused by streamwise vortices originating in the tip region. Farther outboard, both cases display two large skin-friction peaks associated with primary and secondary vortices, as sketched in Fig. 5. These visual patterns

provided a valuable guide to the best locations for laser interferometer measurements.

Axial measurements with the laser interferometer are shown in Figs. 7a-7d. The error bars show the scatter between two or more repeated runs at each location. The data shown include locations of local maximum or minimum shear as determined from the visual patterns. No other measurements or computations were available for comparison because of the impossibility of making such measurements using other methods. However, one might expect a turbulent flat-plate boundary-layer calculation, using the known lee external flow conditions from the tip to the measurement chord to give at least an approximate value for the skin friction on the centerline of the delta wing. The results of such calculations [7] are given in the figures for comparison.

The data for $M_\infty = 2$ and $\alpha = 0°$ are shown in Fig. 7a. This flow is characterized as fairly uniform in the center region, with a small separated region just inboard of the leading edge [8]. The measured skin friction is nearly constant in the center region. It has a narrow peak near the primary vortex and falls off in the separated region. The data show a fairly large scatter at some locations. Possible causes of this are discussed in Sec. 3.4. Also, the peak shear shown at $y/s = 0.75$ could actually be much higher than indicated, because the present delta wing data was not corrected for pressure or shear gradients, and centering the laser on the narrow peak was difficult. In spite of large uncertainties at some locations, the data are seen to be in fairly good agreement with the boundary-layer calculation near the model centerline. But, as expected, the calculation fails farther outboard where the vortex structure dominates the flow field.

If the angle of attack of the delta wing at $M_\infty = 2$ is increased to 8°, the primary vortex grows in size and moves inboard. A counterrotating secondary vortex forms within it [8]. The axial skin friction measured for this case is shown in Fig. 7b. It decreases from the centerline outward, reaching a sharp peak near the primary vortex centerline. It then immediately falls to a very low value at the adjacent separation line and rises to a new lower peak value under the secondary vortex. As in the case at zero angle of attack, the data have a large scatter at some locations. Once again, the data are in fairly good agreement with the boundary-layer calculation near the model centerline.

With the delta wing at $M_\infty = 3$ and $\alpha = 0°$, strong streamwise vortices develop and interfere with the primary vortex on a larger scale than seen at $M_\infty = 2$ [8]. This is reflected in the measured skin friction, as shown in Fig. 7c. From the centerline outward, the skin friction is observed to have several local peaks and valleys with a very large and narrow peak occurring at $y/s = 0.7$, and a low value occurring just inboard of the leading edge. The large peak is probably associated with the primary vortex, but Szodruch [8] was unable to verify its location because of the complex flow structure for this case. The scatter in the data is much less than for $M_\infty = 2$ because the model temperature was measured accurately with a thermocouple for all runs at $M_\infty = 3$. The boundary-layer

calculation is now in excellent agreement with the data on the model centerline.

The skin friction for the delta wing at $M_\infty = 3$ and $\alpha = 8°$ is shown in Fig. 7d. The flow is similar to that at $M_\infty = 2$ at the same angle of attack, in that primary and secondary vortices dominate the structure. Again, the skin friction reaches local peaks under the vortices and falls to a very low value between them at the separation line. The scatter in the data is once again low, and excellent agreement is found with the boundary-layer calculation on the model centerline.

3.4 Sources of Error and Recommendations

The analysis [5] of the data-reduction equations in Appendix A revealed several possible sources of error in the laser interferometer skin-friction method. Assuming a sufficient number of fringes, the single largest source of error is measurement of the distance to the oil leading edge for the single-beam method. The analysis also brought to light some general guidelines on the number of fringes required for accuracy. We found that beyond $\Delta N_2 = 20$, little improvement is gained. Conversely, values less than 10 give significantly less accuracy. Likewise, ΔN_1 should be chosen to be half of the value of ΔN_2. Furthermore, data should preferably be taken late in a run when the oil has thinned to the greatest extent for a maximum ratio of $\Delta t_2/\Delta t_1$. Assuming that these guidelines are satisfied, greater accuracy is achieved by improvements in the method of computing the time increments between fringes. Finally, the analysis showed that it is important to know accurately the viscosity of the oil. Errors can arise from either uncertainties in the viscosity itself, or uncertainties in the oil temperature.

The separated-flow data were generally quite accurate, making large improvements unlikely. The single largest source of error was in the measurement of oil leading-edge distance. That error could be completely eliminated by applying the two-beam method, either using the original near-normal incidence angle method when optical access permits, or by using the new grazing incidence angle method discussed in Appendix B. Beyond that, digital data recording and analysis would offer significant improvements over the manual method used for these tests to determine the time increments between fringes.

In the case of supersonic high-Reynolds-number flow data, there were several sources of error in addition to those mentioned above. The principal error was a result of our inability to record a sufficient number of fringes because of surface waves on the oil. Two solutions to this problem may be possible. We observed that even at the highest skin-friction levels tested, a small region near the oil leading edge always remained wave free, and this region slowly lengthened as the oil thinned. Thus, beam spacing closer than the 5 mm used in these tests should help avoid the waves and allow testing at higher values of skin friction. We also observed that higher viscosity oil helped resist surface waves. Unfortunately, the more viscous oil also required longer run times to obtain an adequate number of fringes. However, the right

combination of oil viscosity and pre-run thinning might allow more fringes or higher skin-friction levels to be attained. In addition to the above source of error, the oil viscosity was poorly known for these tests. The 1,000-cS oil was too viscous to allow the measurement of its viscosity in our gravity-flow experiment [2]. Consequently, we used the nominal value from the Dow Corning product literature.

The tests on the delta wing had several possible sources of error in addition to those already mentioned. In the $M_\infty = 2$ tests, we did not measure the model temperature, assuming it was the same as the tunnel wall. Because we later found that this introduced a significant error, a thermocouple was installed in the model for the $M_\infty = 3$ tests. The reduced scatter in the $M_\infty = 3$ data for which temperature was measured is apparent. As before, a significant source of error also arose from using the single-beam method. The spanwise skin-friction distribution generally had a fine structure, and it was difficult with the single-beam method to exactly relocate a measurement point for repeat measurements. Use of the two-beam method would eliminate this problem. In addition, special care is required to achieve accuracy when testing in regions with large narrow skin-friction peaks. For example, many closely-spaced measurement points may be required to obtain accurately the shear gradients. As before, accuracy would also be enhanced by beam spacing closer than 5 mm. Errors caused by oil streamline curvature and divergence effects would be less, and the correction for shear gradients would be reduced. Finally, applications to larger models would be less sensitive to the error sources described.

4. CONCLUSIONS

The application of a nonintrusive laser-interferometer skin-friction meter has been extended both theoretically and experimentally to several complex wind-tunnel flows. These include two-dimensional separated and reattached subsonic flows with large pressure and shear gradients, as well as two- and three-dimensional supersonic flows at high Reynolds number, including variable wall temperature and cross-flow. In addition, the instrument was shown to provide an accurate location of the mean reattachment length for separated flows. Although some limits to the method for very high skin-friction levels were encountered, levels to 120 N/m^2, or 40 times higher than previous tests, were obtained. The present results establish the utility of this instrument for measuring skin friction in a wide variety of flows of interest in aerodynamic testing.

APPENDIX A: TWO-BEAM SKIN-FRICTION METER DATA-REDUCTION ANALYSIS FOR THREE-DIMENSIONAL FLOW INCLUDING SHEAR-STRESS AND PRESSURE GRADIENTS, WALL-TEMPERATURE VARIATIONS, AND GRAVITY EFFECTS

Consider an oil film with a straight leading edge flowing on a surface subject to shear stress in three-dimensional flow, as shown in Fig. 8. The oil will flow downstream from the leading edge along streamlines aligned with the unknown local surface flow direction. Assume that the focused beams from a two-beam laser interferometer skin-friction meter [2] impinge on the oil at points (1) and (2)

(Fig. 8) located along a line perpendicular to the oil leading edge. Also, assume that the spacing between the beams, Δx, is known and that there is negligible oil streamline curvature or adjacent streamline divergence between the oil leading edge and the measurement points. This can be approximately ensured for most three-dimensional flows by making Δx and the distance from the leading edge to the upstream beam small compared to the streamline radius of curvature. A coordinate system (x,z) is aligned with the oil leading edge, and its origin is arbitrarily placed at the intersection of the streamline through point (1) with the leading edge. A coordinate system (s,n) with the same origin is rotated so that the coordinate s is parallel to the oil streamlines at the unknown oil-flow angle γ. With this geometry, we will develop equations for the two components of skin friction at point (1), namely, τ_{1x} and τ_{1z}. This approach is convenient because one can then position the downstream beam at the exact measurement spot desired.

Tanner and Blows [3] presented a theory that describes the time-dependent thickness of a flowing oil film subject to an arbitrary variation of shear stress, such as that sketched in Fig. 8. By generalizing their analysis to also include an arbitrary variation of oil viscosity with time, it can be shown that the oil-film thickness along a path s for n fixed is given by an integral equation as

$$y(s,n,t) = \frac{\rho}{\sqrt{\tau(s,n)}} \int_0^s \frac{ds}{\sqrt{\tau(s,n)}} \bigg/ \int_0^t \frac{dt}{\nu(t)} \cdot \quad (A1)$$

We now must develop approximate expressions for $\tau(s,n)$ and $\nu(t)$ in terms of known quantities that allow us to integrate Eq. (A1).

The unknown skin-friction distribution $\tau(s,n)$ may be expanded in a Taylor's series about the point (1) as

$$\tau(s,n) = \tau(s_1,o) + \frac{\partial \tau}{\partial s}(s - s_1) + \frac{\partial \tau}{\partial n}(n) + \dots$$

$$\cong \tau_1 + B(s - s_1) + Cn , \quad (A2)$$

with higher-order terms neglected. The unknown shear gradients B and C can be obtained by an iterative procedure to be explained later. Similarly, T(t) is expanded, but only the linear term in temperature is retained so that

$$T(t) \cong T_1 + A(t - t_1') , \quad (A3)$$

where

$$A = (T_2 - T_1)/\Delta t_2 .$$

The notation used is that of a typical two-beam interferometer fringe record, as shown in Fig. 9. The temperature gradient A is determined by direct wall-temperature measurement. Finally, the oil kinematic viscosity variation with temperature can be expressed as

$$\nu(t) = \nu_1 \exp\{-S[T(t) - T_1]\} , \quad (A4)$$

where S is a predetermined constant for each oil.

The integrations in Eq. (A1) may now be carried out through substitution of Eqs. (A2)-(A4). Then following the procedure described in Ref. 2, y can be expressed in terms of a fringe number N, and the concepts of effective fringe number N' and effective oil-flow time t' can be introduced. Then an equation for τ_1 can be written at point (1) in terms of the distance s_1 and the product $N_1't_1'$ at that point. A similar equation for τ_2 at point (2) includes the distance $(s_2 - s_0)$ and the product $N_2't_2'$ at that point. The unknown distances s_1 and $(s_2 - s_0)$ can be obtained in terms of Δx, x_1, and γ from the geometry in Fig. 8. Also, τ_2 can be found in terms of τ_1, B, C, Δx, x_1, and γ by using Eq. (A2) and the geometry in Fig. 8. The expressions for skin friction at points (1) and (2) can be combined to eliminate x_1. The variables N' and t' at each point can be obtained in terms of measured fringe and time increments from fringe records such as in Fig. 9 by using a procedure similar to that in Ref. 2. However, the result is different from that in Ref. 2 because the time increments here must be corrected for variable viscosity through the time integral in Eq. (A1). In addition, if the previously developed correction for pressure gradient and gravity [2] is introduced, a final equation for corrected skin friction at point (1), τ_{1x}', may be written.

The corrected x component of skin friction at point (1) is

$$\tau_{1x}' = \frac{\beta_x}{(1 - \epsilon_x)} \tau_{1x} , \qquad (A5)$$

where τ_{1x} is the uncorrected skin friction given by

$$\tau_{1x} = \frac{2n_0\rho\nu_1 \cos(r)}{\lambda} \cdot \frac{\Delta x}{(N_1't_1' - N_2't_2')} , \qquad (A6)$$

with

$$N_1' = -\Delta N_1 \frac{\dfrac{\Delta N_2}{\Delta N_1}\left(\dfrac{\Delta t_2'}{\Delta t_1'} - 1\right)}{\left(\dfrac{\Delta t_2'}{\Delta t_1'} - \dfrac{\Delta N_2}{\Delta N_1}\right)} ,$$

$$t_1' = -\Delta t_1'\left(\frac{N_1'}{\Delta N_1} + 1\right) , \qquad (A7)$$

$$t_2' = (t_1' + \Delta t_4') ,$$

$$N_2' = -\Delta N_3\left(\frac{t_2'}{\Delta t_3'} + 1\right) ,$$

$$\left.\begin{aligned} \Delta t_i' &= \frac{1}{SA} [\exp(SA \Delta t_i) - 1] \\ &\cong \Delta t_i\left(1 + \frac{1}{2} SA \Delta t_i\right) , \end{aligned}\right\} i = 1,2,4$$

$$(A8)$$

$$\Delta t_3' = \frac{\exp(SA \Delta t_4)}{SA} [\exp(SA \Delta t_3) - 1]$$

$$\cong (1 + SA \Delta t_4)\Delta t_3\left(1 + \frac{1}{2} SA \Delta t_3\right) , \qquad (A8)$$

(concluded)

$$\cos(r) = \cos\left[\text{arc sin} \frac{\sin(i)}{n_0}\right] , \qquad (A9)$$

$$\beta_x = \frac{\left\{1 - \left[\dfrac{\lambda(B \cos^2\gamma - C \sin \gamma \cos \gamma)}{2n_0\rho\nu_1 \cos(r)}\right]\right\}\left\{\times \left[1 - \dfrac{\lambda B}{8n_0\rho\nu_1 \cos(r)} N_2't_2'\right]N_2't_2'\right\}}{\left\{1 - \dfrac{\lambda B}{8n_0\rho\nu_1 \cos(r)} \left[\dfrac{\left(N_1't_1'\right)^2 - \left(N_2't_2'\right)^2}{N_1't_1' - N_2't_2'}\right]\right\}} , \qquad (A10)$$

and

$$\epsilon_x \cong \frac{\lambda\overline{N'}}{2n_0\tau_{1x} \cos(r)} \left[\frac{dp}{dx} - \rho g \sin(\theta),_x\right] . \qquad (A11)$$

In the above, Eq. (A8) represents the integrals of viscosity over time normalized by ν_1 and defined for a general measured time increment, Δt_i. The integrals are also shown expanded in a Taylor's series with only the linear terms retained. This avoids an indeterminate form for the integrals if A is zero. Also, in Eq. (A11), $\overline{N'}$ may be chosen as $(N_1' + \Delta N_2/2)$, and $\rho g \sin(\theta)$, x is the gravity component in the x direction.

Some observations about applying the above data-reduction equations are worth noting. Notice from Eq. (A10) that to minimize the correction for shear gradients the beam spacing and distance from the front beam to the oil-film leading edge should be kept as small as possible, since this reduces the values of $N_1't_1'$ and $N_2't_2'$. In fact, if the single-beam method with the front beam at the oil leading edge is applied, it is easily shown that Eq. (A10) assumes the simple form

$$\beta_x = \frac{1}{\left[1 - \dfrac{B \Delta x}{4\tau_{1x}}\right]} , \qquad (A12)$$

and so $\tau_{1x}' \cong [\tau_{1x} + (1/4)B \Delta x]$. Thus, for this case the uncorrected skin friction is the value located at approximately 75% of the distance from the oil leading edge to the downstream beam, so the correction may be applied by merely shifting the actual measurement point forward from the downstream beam location by the distance $(\Delta x/4)$. The shear-stress gradients, B and C, need not be known at all. No such simple relation exists for the two-beam method, and in that case Eq. (A10) must be applied. Considering Eq. (A11), we note that the pressure gradient and gravity correction can be minimized by waiting for the oil film to thin sufficiently before taking data, since this reduces the value of $\overline{N'}$. Finally, we note that the above set of equations reduces to those in Ref. 2 if the constants A, B, C, and γ are all zero.

If the line of oil shown in Fig. 8 is applied along the x-axis rather than the z-axis, and if the line joining the surface impingement points of the two beams is rotated 90° so that it is parallel to the z-axis, one can show that the instrument will measure the other skin-friction component at point (1), τ'_{1z}. The equations for τ'_{1z} are the same as for τ'_{1x}, except that z replaces x wherever it appears, and the bracketed term involving the angle γ in Eq. (A10) is replaced by $(B \sin^2 \gamma + C \sin \gamma \cos \gamma)$. Once the two skin-friction components at a point are measured, the total skin-friction vector and its direction are obtained.

Application of Eq. (A10) to correct for shear-stress gradients requires that B, C, and γ be determined by an iterative procedure that should converge for small corrections. Initial values for these constants may be estimated from plots of the uncorrected skin-friction components as computed from Eq. (A6).

APPENDIX B: DESCRIPTION OF A GRAZING INCIDENCE ANGLE TWO-BEAM SKIN-FRICTION METER

The two-beam skin-friction meter uses beams with two orthogonal polarizations to allow signal separation. The polarization with the electric vector perpendicular to the incidence plane is commonly denoted as the s polarization, and its normal is the p polarization. The surface reflectance for these polarizations is shown as a function of incidence angle for silicon oil and polished steel in Fig. 10 [9]. For the previous application of the instrument [2], incidence angles near 0° were used; one can see that the oil reflects about 3% of the light for both polarizations. This was sufficient for good signal modulation on the recorded fringe records, even though the optimum would be to have the oil and substrate reflectances equal. One can see that for the present test with incidence angles near the Brewster angle of 54°, the oil reflects the p polarization poorly. Insufficient signal modulation results, making the two-beam method unsuitable.

However, the use of a grazing incidence angle close to 90° will restore the p-polarized beam reflectance and provide both s and p reflectances nearly equal to that of a metal substrate (see Fig. 10). We successfully demonstrated this technique for an incidence angle of 80°, obtaining excellent fringe records for both beams. The only stringent new requirements were (1) that the substrate surface have a very good polish, because much of the beam interference now comes from multiple reflections between the oil and the substrate; and (2) that care be taken in focusing the beam to avoid elongation in the incidence plane and any resultant degradation of fringe contrast as a result of the beams crossing more than one fringe. On the other hand, an incidence angle close to 90° has several advantages over smaller angles. For example, most wind-tunnel test sections have easier optical access from the sides than they do from the top. Furthermore, the oil reflectivity can be controlled to more closely match the substrate for optimum fringe contrast by changing the incidence angle slightly. Finally, the refraction angle in the oil is close

to its asymptotic value, thus easing the accuracy requirements on measuring the beam incidence angle.

REFERENCES

1. Winter, K. G., "An Outline of the Techniques for the Measurement of Skin Friction in Turbulent Boundary Layers," Progress in the Aerospace Sciences, Vol. 18, Pergamon Press, Great Britain, 1977, pp. 1-57.

2. Monson, D. J. and Higuchi, H., "Skin Friction Measurements by a Dual-Laser-Beam Interferometer Technique," AIAA Journal, Vol. 19, No. 6, June 1981, pp. 739-744.

3. Tanner, L. H. and Blows, L. G., "A Study of the Motion of Oil Films on Surfaces in Air Flow, with Application to the Measurement of Skin Friction," Journal of Physics E: Scientific Instruments, Vol. 9, No. 3, Mar. 1976, pp. 194-202.

4. Tanner, L. H., "A Skin Friction Meter, Using the Viscosity Balance Principle, Suitable for Use with Flat or Curved Metal Surfaces," Journal of Physics E: Scientific Instruments, Vol. 10, No. 3, Mar. 1977, pp. 278-284.

5. Kline, S. J. and McClintock, F. F., "Describing Uncertainties in Single-Sample Experiments," Mechanical Engineering, Vol. 75, No. 1, Jan. 1953, pp. 3-8.

6. Sindir, M., "Study of Turbulent and Laminar Recirculating Flows in a Backward-Facing Step Geometry," Doctoral Dissertation, Mechanical Engineering Dept. U. of California at Davis, Davis, Calif. (to be published in 1982).

7. Tong, H., Buckingham, A. C., and Curry, D. M., "Computational Procedure for Evaluations of Space Shuttle TPS Requirements," AIAA Paper 74-518, 7th Fluid and Plasmadynamics Conference, Palo Alto, Calif., 1974.

8. Szodruch, J., "Experimental Study of Viscous Leeside Flow Over a Slender Delta Wing," NASA TM-81248, 1980.

9. Jenkins, F. A. and White, H. E., Fundamentals of Optics, 3rd ed., McGraw-Hill, New York, N. Y., 1957.
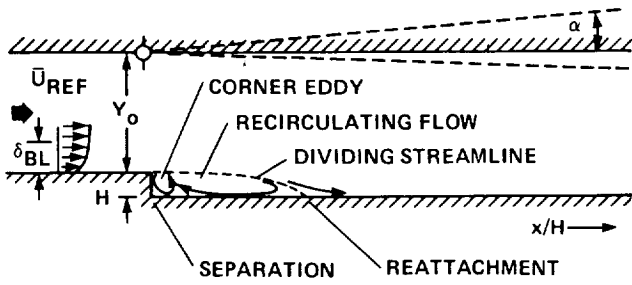
Fig. 1 — Rearward-facing step-flow experimental geometry and inlet conditions. Tunnel geometry: H = 1.27 cm, Y_O = 8H, tunnel span = 12H, $-2° \leq \alpha \leq 10°$. Inlet conditions: $\bar{U}_{REF}$ = 44.2 m/sec, $M_{\infty,REF}$ = 0.128, δ_{BL} = 1.9 cm, R_θ = 5,000.

(a) α = 0°
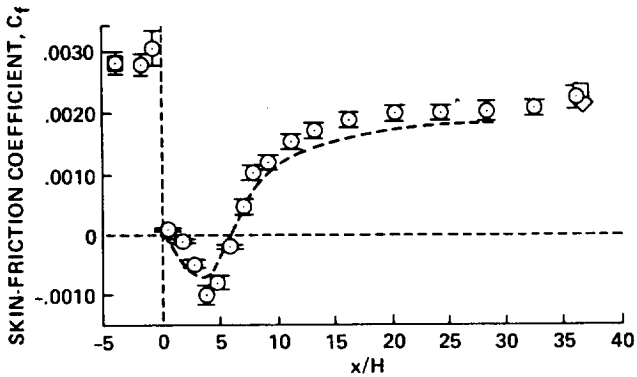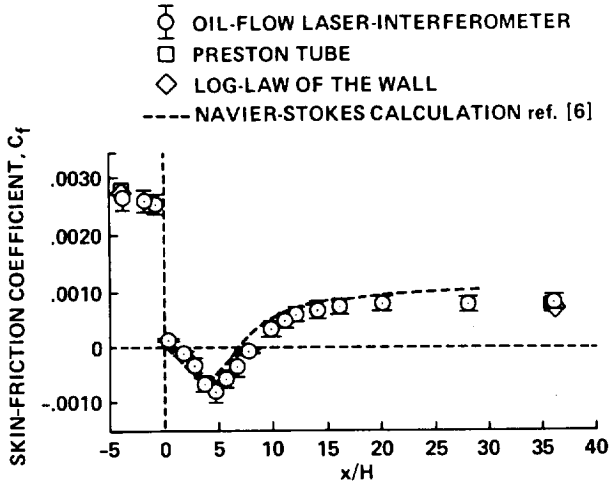
(b) α = 6°

Fig. 2 — Skin friction measured over a rearward-facing step with separation.
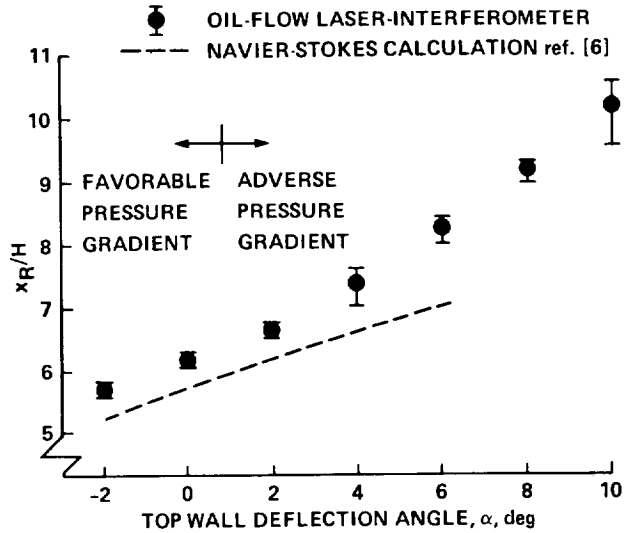
Fig. 3 — Reattachment location vs top-wall deflection angle.
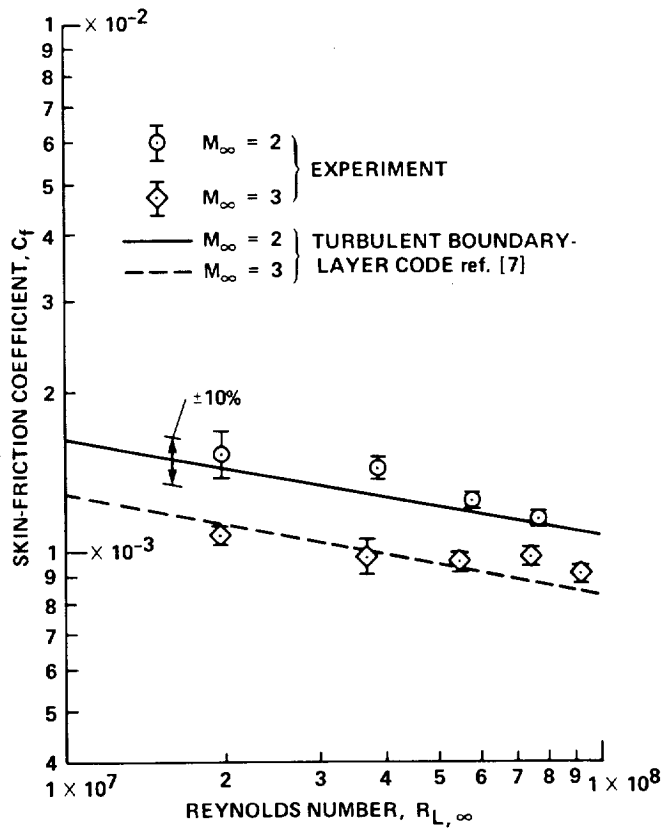
Fig. 4 — Wall skin friction measured at supersonic Mach numbers.
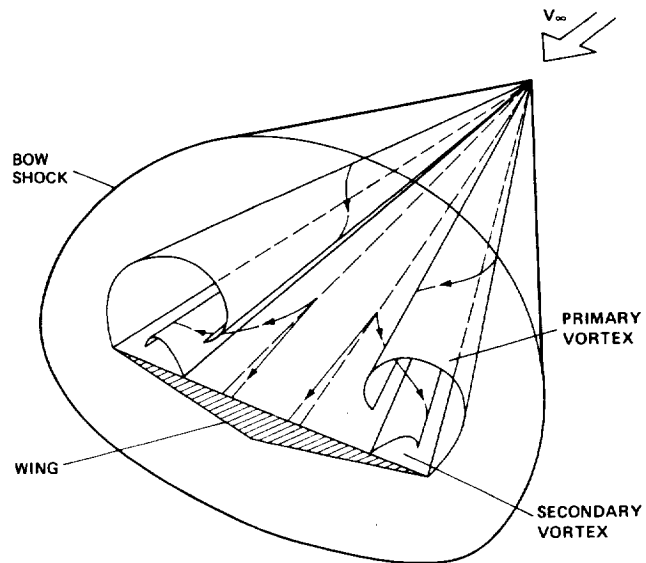
Fig. 5 — General features of the supersonic lee
flow over a delta wing at angle of attack.

(a) $M_\infty = 2$

(b) $M_\infty = 3$
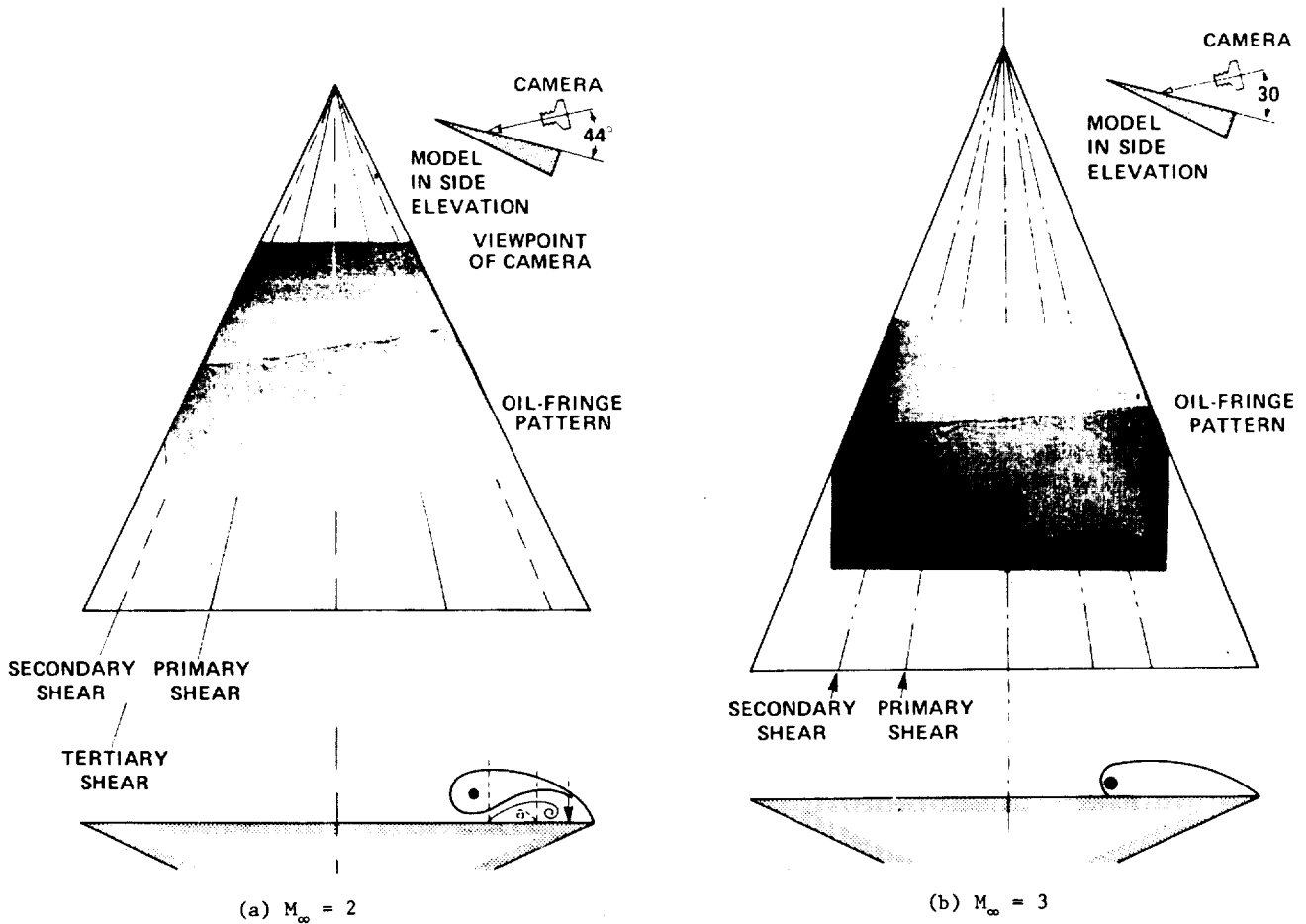
Fig. 6 — Skin friction fringe pattern on lee of delta wing at $\alpha = 8°$ and $R_{L\infty} = 2.0 \times 10^6$ (oil lines slightly skewed from direction normal to tunnel flow).
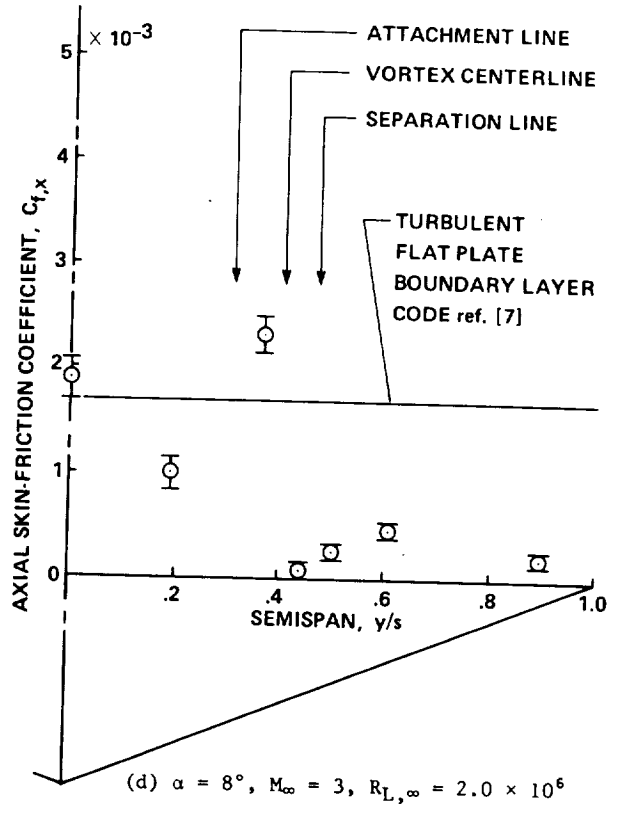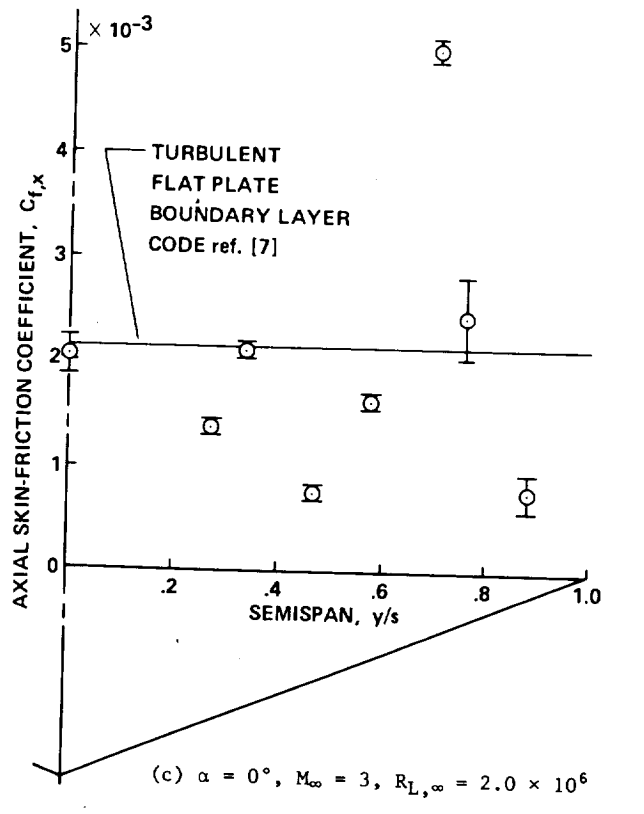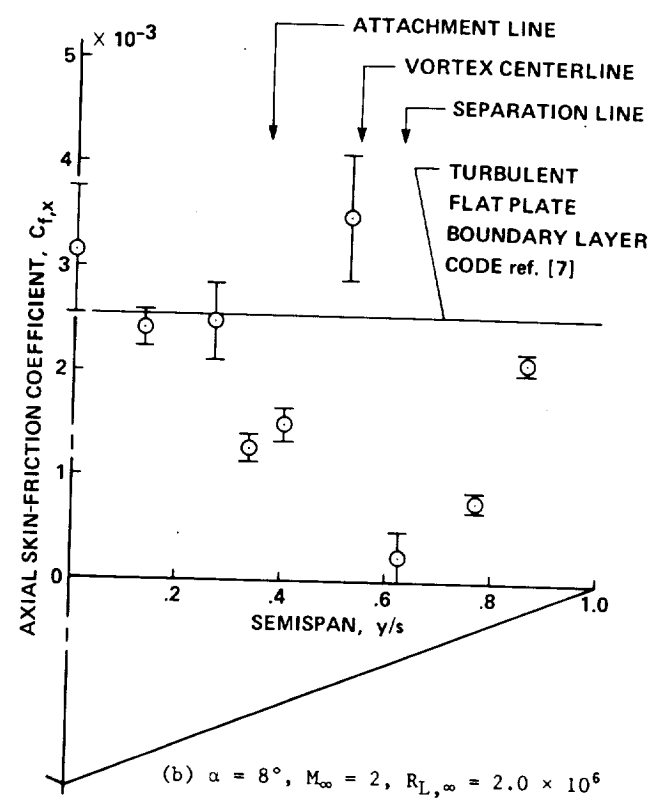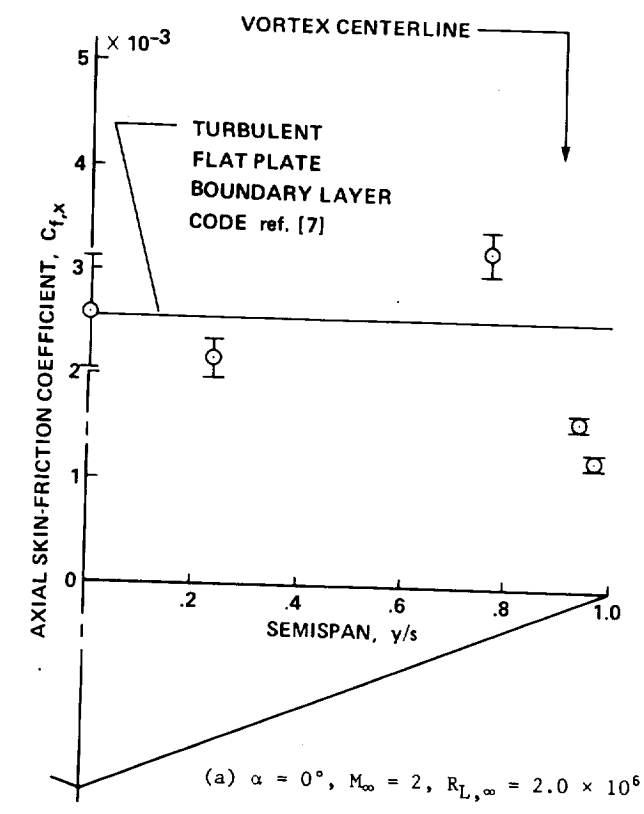
Fig. 7 — Skin friction measured on the lee of a delta wing.

Fig. 8 — Geometry and notation for application of a two-beam, laser-interferometer skin-friction meter in three-dimensional flow.

Fig. 9 — Typical fringe record from a wind-tunnel test of a two-beam, laser-interferometer skin-friction meter; beam spacing is 5 mm.

Fig. 10 — Surface reflectance [9] for silicon oil (Eq. 25a) and polished steel (approx.) at 6328 Å vs incidence angle.